Vibrational dynamics of filled skutterudites $M_{1-x}Fe_4Sb_{12}$ (M=Ca, Sr, Ba, and Yb)

Michael Marek Koza,[1,2] Lucia Capogna,[1,3] Andreas Leithe-Jasper,[2] Helge Rosner,[2] Walter Schnelle,[2] Hannu Mutka,[1] Mark Robert Johnson,[1] Clemens Ritter,[1] and Yuri Grin[2]

[1]*Institut Laue Langevin, 6 Rue Jules Horowitz, BP 156, 38042 Grenoble Cedex 9, France*

[2]*Max-Planck-Institut für Chemische Physik fester Stoffe, Nöthnitzer Straße 40, 01187 Dresden, Germany*

[3]*CRS-SOFT and OGG Grenoble, CNR-INFM, 6 Rue Jules Horowitz, 38042 Grenoble Cedex 9, France*

(Received 28 October 2009; revised manuscript received 17 March 2010; published 5 May 2010)

First-principles density-functional theory and lattice-dynamics calculations were performed to study the vibrational dynamics and related observables of the ternary compounds $Ca_{1-x}Fe_4Sb_{12}$, $Sr_{1-x}Fe_4Sb_{12}$, $Ba_{1-x}Fe_4Sb_{12}$. and $Yb_{1-x}Fe_4Sb_{12}$. The calculation results are supported by experimental data, which were obtained from neutron inelastic scattering, neutron-diffraction, and heat-capacity measurements. Within the calculation approach based on the theory of harmonic solids all observables are linked to the phonon density of states $Z(\omega)$. The good agreement with experimental data shows that the vibrational dynamics of the ternary skutterudite structures can be described by a set of normal modes. Features in the experimentally obtained density of states $G(\omega)$ reflecting the variation in properties (mass, ionic radius) of the cations Ca, Sr, Ba, and Yb are reproduced by the calculations. The quality of the inelastic neutron experiments enables the detection of at least two mode peaks at 4.9 and 5.7 meV with a pronounced spectral weight of ytterbium.

DOI: 10.1103/PhysRevB.81.174302 PACS number(s): 63.20.dd, 63.20.Pw, 61.05.fg

I. INTRODUCTION

Compounds commonly referred to as skutterudites have the composition TX_3 (space group $Im\bar{3}$) with transition-metal atoms (T=Co,Rh,Ir) forming a simple cubic lattice. Three out of four of the cubes spanned by the T atoms are occupied by nearly rectangular rings of four pnictogens (X=P,As,Sb).[1,2] The empty cubes can be gradually "filled" with electropositive elements M (e.g., alkaline-earth, rare-earth, actinide atoms, or thallium) when electronic compensation is performed substituting T=Co,Rh,Ir by T=Fe,Ru,Os, respectively.[3] The stoichiometry of the ternary skutterudites, which we refer to as the filled skutterudites in the following, can be represented as $M_{1-x}T_4X_{12}$ and two common representations of its structure are sketched in Fig. 1.

In recent years skutterudite compounds have been in the focus of material research for thermoelectric applications.[4–6] The reason is that in the process of progressively filling the empty binary skutterudite its lattice thermal conductivity undergoes a strong reduction which is a prerequisite for thermoelectric materials with a high figure of merit.[7–9] For example, filling the $CoSb_3$ structure with Ce reduces the thermal conductivity by more than one order of magnitude at about half-filled stage.[10,11] When a complete filling is achieved in the structure $Ce_{1-x}Fe_4Sb_{12}$ the thermal conductivity still remains reduced by a factor of 6–7 at room temperature.

Slack *et al.*[12] conjectured that large vibrational amplitudes of the encaged cations, frequently referred to as "rattling" in the literature, initiate an additional, dynamic scattering mechanism for the heat-carrying acoustic phonons, thus, reducing their mean-free path l_{mfp} and perturbing the thermal conduction efficiently. In a congruent way, resonant scattering of acoustic phonons at localized "rattling" modes has been proposed as a reduction mechanism of l_{mfp} in clathrates and clathrate hydrates.[13–15] Support for this resonant scattering hypothesis could be given by computation of the interaction of acoustic phonons in methane clathrate hydrate.[16,17] On the basis of structural studies indicating augmented atomic displacement parameters (ADP) of the M atoms and of specific-heat data analysis the presence of additional modes at low frequencies in filled skutterudites was deduced.[5,18–20] Low-resolution spectroscopic studies have indeed given evidence of an excess of inelastic intensity at low energies often referred to as Einstein modes[21–26] and a recent spectroscopic study of Misch-Metal skutterudites[27] points at a pronounced interaction of the cations with the anion lattice, although, only higher-energy modes could be probed by the applied technique. Consequently, some experimental support for the resonant scattering of acoustic phonons at "rattling" ions M might be surmised.

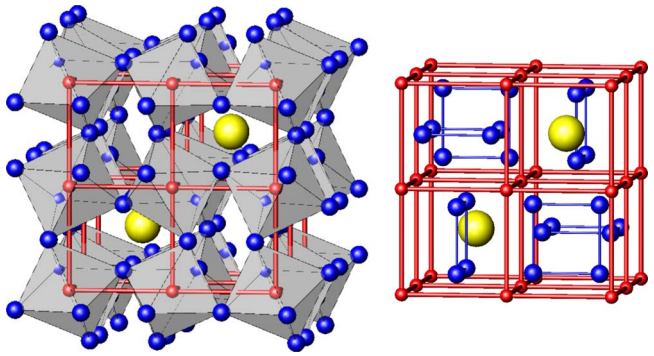

FIG. 1. (Color online) Two common presentations of a filled skutterudite structure MT_4X_{12} (space group $Im\bar{3}$). Yellow (large) spheres represent the cations M, red (small) and blue (intermediate size) spheres indicate T and X positions, respectively. Sketch on the left-hand side stresses the X octahedra surrounding the T sites. Sketch on the right-hand side, indicates the X rectangles, which occupy three out of four of the cube cavities formed by the T network.

However, inconveniences of the "rattler" concept become obvious when properties that depend on the dynamic response are inspected in detail. Schnelle *et al.*[20] have shown recently that the frequencies of Einstein modes deduced from ADPs cannot be brought into agreement with those deduced from specific-heat measurements for a number of M atoms in $M_{1-x}Fe_4Sb_{12}$ compounds. Although, light-weight cations such as sodium, potassium, and calcium appear to be strong "rattlers" and even cations of moderate and heavy mass such as strontium and barium appear to "rattle" moderately, their "rattling" dynamics does not seem to constitute the leading term in the compounds' thermodynamic observables, e.g., in the specific heat.

Feldman *et al.*[28–31] presented extensive work on the lattice dynamics of empty $CoSb_3$ and La- and Ce-filled Fe_4Sb_{12} compounds based on experiments and computational approaches. The authors have carefully commented that the "… simplest "rattling" models are inapplicable to these filled skutterudites, …"[29] Strong hybridization of vibrational modes of the cations with strongly Sb-weighted modes has been conjectured which should result in a pronounced renormalization of the low-energy frequency spectrum. Congruent conclusions on the hybridization of vibrational modes of thallium cations with Sb-weighted modes have been drawn from *ab initio* calculations by Ghosez *et al.*[32] for $TlFeCo_3Sb_{12}$.

Having applied high-resolution inelastic neutron scattering (INS) Koza *et al.*[33,34] have shown that *ab initio* density-functional theory (DFT) and lattice-dynamics calculations, whose results are in full accordance with the data of Feldman *et al.*, are capable of reproducing the inelastic response of the La- and Ce-filled $M_{1-x}Fe_4Sb_{12}$ compounds to a high degree. A pronounced renormalization of eigenfrequencies has been established, resulting in the presence of at least two La/Ce-weighted mode bands centered at 5.5 meV (64 K) and 7.3 meV (85 K) in the vibrational density of states and not being visibly affected by temperature variation between 2 and 600 K. Moreover, the experimentally obtained dynamic structure factor $S(Q,\omega)$, i.e., the momentum Q and energy $\hbar\omega$-dependent intensity profile, has been adequately approximated by powder-averaged lattice-dynamics calculations. Consequently, La- and Ce-filled iron antimonides appear to be quasiharmonic crystalline compounds whose low-energy dynamic is characterized by complete hybridization of cation and Sb vibrational modes leading to an extended symmetry-avoided anticrossing of eigenmodes of acoustic and optic character.[35,36] Equivalent conclusions have been drawn from INS and inelastic x-ray scattering experiments on single crystals of $CeOs_4Sb_{12}$,[37,38] $CeRu_4Sb_{12}$,[39] $PrRu_4Sb_{12}$ and $PrOs_4Sb_{12}$,[40,41] and $SmRu_4P_{12}$.[42] Thus, the applicability of the concept of reduced lattice thermal conductivity as a resonance effect of acoustic phonons with "rattling" cations is not readily obvious in the case of the filled skutterudites, while all skutterudite materials showed a pronounced symmetry-avoided anticrossing of phonon modes, praseodymium-containing compounds displayed in addition some phonon softening upon cooling. Note that such a redshift on cooling and, hence, blueshift on heating is captured by the generic picture of a U-shaped bonding potential of the M atoms in which at elevated temperatures the quartic and higher-order terms of a symmetric potential become evident.[34] Examples of such anharmonic frequency shift are reported for $RGa_{16}Ge_{30}$ (R=Sr,Ba,Eu) clathrates[43,44] and have been established as an extreme effect in N_2-filled clathrate hydrates[36,45] as well as in MOs_2O_6 (M=K,Rb,Cs).[46] Thus, it is obvious that the notion of "rattling" does not characterize globally the inelastic properties of M atoms as was shown by the experiments of Schnelle *et al.*[20] In addition, the perception of quasiharmonicity needs to be inspected and verified specifically for different skutterudite compounds as long as a systematic trend in the variation in inelastic properties upon a variation in the M atom and of the TX_3-lattice constituents has not been unequivocally established.

The aim of the present study is to explore a possible systematic tendency in the dynamic properties of filled skutterudites $M_{1-x}Fe_4Sb_{12}$ and to shed light on the effect of the M-cation variation in the sequence Ca, Sr, Ba, and Yb. We focus here on the vibrational density of states and related observables resulting from *ab initio* lattice-dynamics calculations and verified in experiments. The experimentally obtained specific heat data have been reported in Ref. 20 and are reexamined here for comparison with the lattice dynamics calculations results. Forthcoming publications will present temperature response and dispersive properties of the vibrational dynamics as well as details of the calculation techniques.

The paper is structured as follows. The next section presents the details of the calculations and the experimental techniques applied. We proceed with a presentation of the calculated potentials and of the thermal parameters as obtained from calculation and Rietveld fits to diffraction data. An extensive and detailed report of vibrational dynamics follows, however, limited to information on the vibrational density of states of the compounds obtained from time-of-flight neutron-scattering measurements and lattice-dynamics calculations. The data presentation is completed by a discussion of specific-heat results from experiments and calculations. We finish by a general discussion of the computed and experimental data.

II. CALCULATION AND EXPERIMENTAL TECHNIQUES

A. *Ab initio* lattice-dynamics calculations

Electronic and ionic first-principles calculations were performed using the projector-augmented wave formalism[47] of the Kohn-Sham DFT (Refs. 48 and 49) at the generalized gradient approximation (GGA) level, implemented in the Vienna *ab initio* simulation package (VASP).[50,51] The GGA was formulated by the Perdew-Burke-Ernzerhof[52,53] density functional. The Gaussian broadening technique was adopted and all results are well converged with respect to k mesh and energy cutoff for the plane-wave expansion. As introduced in Ref. 34 the supercell applied in the present calculation comprised two structural units (34 atoms) and the results can be, hence, compared with the data for $LaFe_4Sb_{12}$. For any compound restoring forces were verified to drop off by at least 3 orders of magnitude within the supercell.

TABLE I. Nuclear coherent σ_{coh} and incoherent σ_{inc} neutron scattering cross sections in barns, mass M in atomic mass unit and ionic radii in angstrom of the studied skutterudite elements. Ionic radii are taken for a coordination number VIII from Ref. 61. The effective scattering power σ_{tot}/M is given in barns/amu $\times 10^3$.

Element	σ_{coh}	σ_{inc}	σ_{tot}	M	σ_{tot}/M	Radius
Fe	11.22	0.4	11.62	55.8	208.2	
Sb	3.9		3.9	121.8	32.0	
Ca^{+2}	2.78	0.05	2.83	40.1	70.6	1.26
Sr^{+2}	6.19	0.06	6.25	87.6	71.3	1.40
Ba^{+2}	3.23	0.15	3.38	137.3	24.6	1.56
Yb^{+2}	19.42	4	23.4	174.0	134.5	1.28

Following geometry optimization, a series of single point energy calculations, which give the Hellmann-Feynmann forces acting on all atoms in the cell, were performed on the structures obtained by displacing, one at a time, each of the inequivalent atoms in positive and negative Cartesian directions. The dynamical matrix for any point in reciprocal space was then generated and diagonalized in the program PHONON,[54] which thereafter allows dispersion curves, vibrational densities of states, heat-capacity, and mean-square displacement to be calculated. This method of calculating phonons is referred to as the direct method or supercell approach.[55]

In order to calculate the coherent neutron-scattering function for the powder samples, which will be discussed in a forthcoming publication, we have adapted the dispersion curve calculation in PHONON, which also gives the coherent structure factor, for randomly chosen wave vectors rather than wave vectors along high symmetry directions (see Refs. 33, 34, and 56). The spectral frequencies and intensities are then computed according to energy and momentum transfer to generate the $S(Q,\omega)$ map.

B. Experimental procedure

Four samples of the respective compositions $M_{1-x}Fe_4Sb_{12}$ with M=Ca, Sr, Ba, Yb were prepared following the sample preparation procedure reported in detail in previous publications.[20,57] The samples were studied by neutron time-of-flight spectroscopy and neutron diffraction. The cold neutron time-of-flight spectrometer IN6@ILL, located at the European neutron source Institut Laue Langevin in Grenoble, France, has been used to measure the inelastic signals of the samples at room temperature. IN6@ILL has been exploited with a neutron incident wavelength of 4.14 Å and the time-focusing mode with the best energy resolution set at 7 meV. This time-focusing setup allows a sampling of the dynamics on the anti-Stokes line with a relative energy resolution of about 2% and, hence, a monitoring of guest modes below 10 meV with a resolution better than 200 μeV and of the Fe dynamics around 30 meV with a resolution of 500–800 μeV (for the resolution of a comparable setup see Ref. 58).

The recorded response has been corrected for empty sample holder scattering and a smooth background and normalized to a vanadium standard to account for different detector efficiencies. Conversion of the signal to the so-called generalized density of states $G(\omega)$ was performed within the incoherent approximation following established mathematical relations.[46,59,60] Table I reports the scattering cross sections σ, their masses (amu) and the resulting scattering powers σ/amu of the samples' constituents. Note that despite the variation in the scattering powers of the elements, which results in an intensity modification of $G(\omega)$ in respect to the vibrational density of states $Z(\omega)$, the almost identical scattering powers of Ca, Sr as well as La (Ref. 34) allows an accurate comparison of the guest mode intensities.

With due care to the complex electronic structures depending on the encaged cations, in a simplified scenario we may expect to gain information about the mass effect by comparing the results of Ca and Yb cations being approximately of the same size. Indeed, it has been experimentally and theoretically shown that the Ca- and Yb-filled iron antimonides have a very similar electronic structure.[57] The effect of the cation size on the dynamics of the compounds can be studied by comparing, for example, results from experiments on Ba and La cations which have approximately the same mass.[34] Specific-heat measurements to which we refer to here were reported by Schnelle *et al.* in full detail in Refs. 20 and 57.

Temperature-dependent diffraction data of all four samples have been recorded with the high-resolution diffractometer D2B@ILL of the Institut Laue Langevin. An incident wavelength of 1.0510 Å and the highest flux setup resulting in a natural collimation of the incident beam of 27′ was applied. Standard equipment, i.e., cylindrical vanadium sample holders with a diameter of 7 mm and cryostats, were utilized. Diffraction patterns were recorded at 3, 20, 80, 140, 200, and 295 K. The entire suite of data was collected in two runs comprising Ca-, Sr-, and Ba-containing iron antimonides in the first and $Yb_{1-x}Fe_4Sb_{12}$ in the second run. The $Yb_{1-x}Fe_4Sb_{12}$ measurements were performed in a cryostat contributing two pronounced peaks at about 26° and 30°. Those peaks were suppressed in the data analysis [Rietveld refinement with the software package FULLPROF (Ref. 62)]. The occupancy of the M sites was freely fitted in the analysis. Within the entire set of results taken at different temperatures its value scattered between 94% and 98% (x =0.06–0.02) for any of the M cations.

III. RESULTS

A. Observables related to the dynamic response

Despite the diversity of observables discussed in the present paper these observables can be related to the vibrational density of states of the material following the theory of harmonic crystals[63]

$$Z(\omega) = \sum_i Z_i(\omega), \tag{1}$$

with $Z_i(\omega)$ denoting the partial contributions by M, Fe, and Sb atoms.

Harmonicity implies that the mean-square displacement of the material constituents $\langle u_i^2(T)\rangle$ and, hence, the ADPs (for the isotropic case $U_{\mathrm{iso}}(T)=1/3\cdot\langle u_i^2(T)\rangle$) can be approximatively related to $Z_i(\omega)$ as

$$\langle u_i^2(T)\rangle = \frac{3}{2}\frac{\hbar}{M_i}\int \frac{Z_i(\omega)}{\omega}\coth\left(\frac{\hbar\omega}{2k_{\mathrm{B}}T}\right)d\omega, \tag{2}$$

in which M_i is the mass of the scatterer and k_{B} is the Boltzmann constant. Equation (2) explicitly accounts for three normal modes per atom with a density of states normalized to unity $\int Z_i(\omega)d\omega=1$. When presenting the density of states $Z(\omega)$ in Sec. III C we will apply this normalization to any atom of the structural unit resulting, hence, in 51 normal modes for the filled structures. $\langle u_i^2(T)\rangle$ can be asymptotically approximated for low and high temperatures as

$$\langle u_i^2(T)\rangle_{T\to 0} = \frac{3}{2}\frac{\hbar}{M_i}\cdot\int \frac{Z_i(\omega)}{\omega}d\omega, \tag{3}$$

$$\langle u_i^2(T)\rangle_{T\to\infty} = 3\frac{k_{\mathrm{B}}T}{M_i}\cdot\int \frac{Z_i(\omega)}{\omega^2}d\omega. \tag{4}$$

As a consequence, the mean-square displacement is expected to crossover from a constant value at low temperatures determined by the quantum-mechanical zero-point oscillations to a behavior $\propto T$ upon heating.

Approximating the density of states by Einstein's single oscillator model $Z_i(\omega)=\delta(\omega-\omega_{i,\mathrm{E}})$ with $\hbar\omega_{i,\mathrm{E}}=k_{\mathrm{B}}\Theta_{i,\mathrm{E}}$ reduces Eq. (2) to the simple relation

$$\langle u_i^2(T)\rangle = \frac{3}{2}\frac{\hbar}{M_i}\cdot\frac{1}{\omega_{i,\mathrm{E}}}\cdot\coth\left(\frac{\hbar\omega_{i,\mathrm{E}}}{2k_{\mathrm{B}}T}\right), \tag{5}$$

which was used for estimating the cation Einstein frequency from the ADP of diffraction data reported in Table VI.

An estimation of the eigenfrequencies $\omega_{i,\mathrm{R}}(\vec{r})$ of the cation excitations can be as well computed from the DFT energy calculation as

$$K_i(\vec{r}) = -\partial^2 V_i(\vec{r})/\partial\vec{r}^2 = M_i\omega_{i,\mathrm{R}}^2(\vec{r}) \tag{6}$$

with $V_i(\vec{r})$ the potential energy and $K_i(\vec{r})$ the constant of the restoring force. The $\omega_{i,\mathrm{R}}(\vec{r})$ (Table VI) was computed in the high symmetry direction [1,0,0].

Heat capacity can be as well linked to the density of states and by applying the approximation $C(T)=C_p(T)\approx C_V(T)$ we obtain

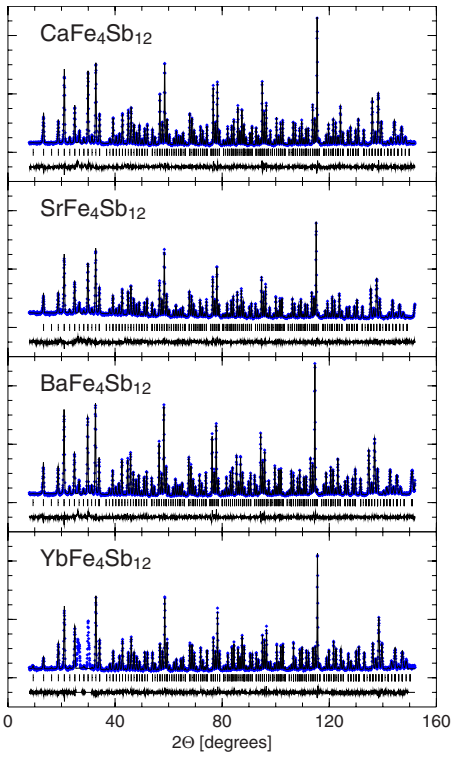

FIG. 2. (Color online) Neutron-diffraction data of the four skutterudite compounds indicated in the figure. Data are obtained at $T=3$ K and $\lambda=1.0510$ Å at the diffractometer D2B@ILL. Rietveld refined diffraction profiles are plotted as full lines with the experimental data points and the respective difference signal between experimental and refined data is plotted below. Short vertical lines above the difference signal mark the Bragg-peak positions.

$$C_i(T) \approx 3k_{\mathrm{B}}\int \left(\frac{\hbar\omega}{k_{\mathrm{B}}T}\right)^2 \frac{Z_i(\omega)}{\sinh^2\left(\frac{\hbar\omega}{2k_{\mathrm{B}}T}\right)}d\omega \tag{7}$$

with

$$C(T) = \sum_i C_i(T). \tag{8}$$

The calculated values of $C(T)$ reported in Sec. III E were normalized to the total specific heat $c(T)$ to match the units of the measurements in Refs. 20 and 64.

B. Experimental diffraction pattern, thermal displacement parameters, and calculated potentials

Let us begin the data presentation with results from the *ab initio* calculations which can be linked to diffraction data. Figure 2 shows the diffraction patterns obtained from D2B@ILL experiments together with the calculated and difference patterns. Tables II and III report the lattice parameters and the refined position parameters of Sb.

A correspondence between the magnitude of the lattice parameter and the guest size is found. An excess of the calculated lattice parameters can be reported in all structures reaching a relative maximum deviation of less than 0.5% when compared with experimental data taken at 3 K. Barium

TABLE II. Lattice parameters obtained from *ab initio* calculations (calc.) and Rietveld refined neutron-diffraction data at the given temperatures T. Fitted parameters are given with FULLPROF standard deviations.

T/K	Ca	Sr	Ba	Yb
Calc.	9.187	9.210	9.240	9.176
3	9.1401(2)	9.1597(5)	9.1822(2)	9.1352(4)
20	9.1399(2)	9.1597(5)	9.1822(2)	9.1332(4)
80	9.1422(2)	9.1615(5)	9.1843(2)	9.1354(4)
140	9.1473(2)	9.1664(5)	9.1892(2)	9.1405(4)
200	9.1528(2)	9.1723(6)	9.1946(2)	9.1464(4)
295	9.1630(2)	9.1817(6)	9.2054(2)	9.1568(5)

as the largest M cation demands the largest cavities and, hence, the largest lattice. The relative changes in the lattice parameters as well as the fractional parameters of the Sb atoms calculated and obtained from Rietveld refinement are in good agreement. Comparison of experimentally found and calculated interatomic distances reveal a 2% larger Sb-Sb distance in calculations and almost no difference for the Fe-Sb distances.

Some selected potentials and restoring forces which result from the *ab initio* calculated atomic arrangement are reported in Fig. 3. Restoring forces obtained from fits of a harmonic (quadratic) potential to data for displacements of up to ± 0.15 Å are listed in Table IV. The results of the quadratic fits to the M-cation potentials are indicated by solid lines in Fig. 3.

There are four obvious conclusions that can be drawn from the entire body of the potential data. (1) The M-cation potentials are to a good approximation harmonic $\propto \Delta x^2$ within the calculated limits. (2) The force constant of restoring forces acting at the M cations follow the trend of the cation radius size. (3) Cation and Fe potentials are moderately orientation dependent with a force constant decreasing by about 20% with respect to [100], [110], and [111] directions. These data are not shown here. (4) Due to site symmetry, Sb potentials are highly anisotropic and anharmonic with respect to [100], [010], and [001] directions. In $Ba_{1-x}Fe_4Sb_{12}$ the directional force constant of Ba approaches values of the Sb force constant.

Figure 4 reports the isotropic ADPs $U_{iso}(T)$ obtained from the *ab initio* lattice-dynamics calculations and the powder neutron-diffraction experiments. An excellent agreement can be found in the $U_{iso}(T)$ values of the cations as well as the Fe and Sb data. Here not only the relative properties are reproduced but a good correspondence is found also on an absolute scale. Note that this correspondence comprises the zero-point oscillations at $T=3$ K as well as the dependence upon temperature changes. Consequently, up to about 300 K all sample constituents follow the behavior approximated for a harmonic sample expressed by Eq. (2).

TABLE III. Fractional position parameter of Sb obtained from *ab initio* calculations ($0yz$) and Rietveld refined neutron-diffraction data ($0y'z'$) at $T=3$ K.

	Ca	Sr	Ba	Yb
y	0.162	0.163	0.164	0.162
z	0.334	0.336	0.338	0.333
y'	0.1596(1)	0.1601(2)	0.1614(1)	0.1598(2)
z'	0.3368(1)	0.3380(2)	0.3401(1)	0.3366(4)

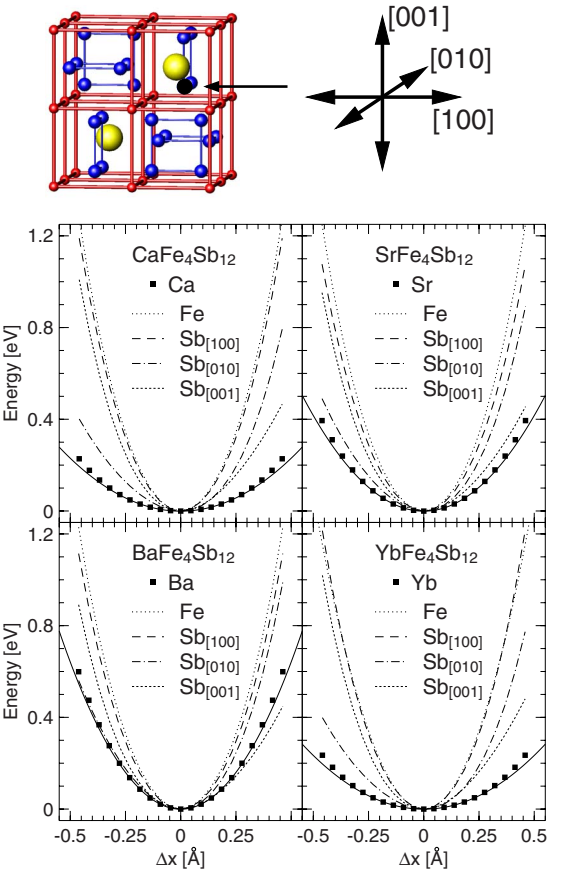

FIG. 3. (Color online) Potential energy calculated for Ca-, Sr-, Ba-, and Yb-filled skutterudites. The M cation and the corresponding Fe potentials are shown for the [100] direction exclusively. Sb potentials are calculated for [100], [010], and [001] directions highlighting the strong anisotropy and the dependence on the M-cation size. The calculations were performed for a discrete grid of displacements. Solid data points exemplify this grid for the M-cation results. Full lines plotted with the cation potentials correspond to quadratic fits to the data in the range ± 0.15 Å. All other lines represent the DFT calculated potentials explained in more detail in the text. Sketches on top indicate the orientation of the structure and the reference Sb site.

C. Vibrational properties and phonon density of states

Figure 5 reports the calculated phonon density of states $Z(\omega)$ for the studied filled skutterudites and for the empty compound $CoSb_3$. The low-energy region of $Z(\omega)$ determines substantially the ADPs and heat capacity of the materials via Eqs. (2) and (7) (Fig. 5, right). The total $Z(\omega)$ (black in Fig. 5) is normalized to 51 modes (48 modes in $CoSb_3$ adapting the stoichiometry to the ternary skutterudites as

TABLE IV. Restoring forces in electron volt per square angstrom of the sample constituents from fits of a harmonic potential to data reported in Fig. 3 in the range $\Delta x=[-0.15,0.15]$ Å. Force directions are indicated with the element symbols.

Compound	$M_{[100]}$	$Fe_{[100]}$	$Sb_{[100]}$	$Sb_{[010]}$	$Sb_{[001]}$
$Ca_{1-x}Fe_4Sb_{12}$	0.89	5.30	4.93	2.47	3.17
$Sr_{1-x}Fe_4Sb_{12}$	1.63	5.20	4.45	2.89	3.00
$Ba_{1-x}Fe_4Sb_{12}$	2.52	5.09	4.54	3.27	2.82
$Yb_{1-x}Fe_4Sb_{12}$	0.90	5.36	5.03	2.43	3.24

Co_4Sb_{12}) accounting for three degrees of freedom per atom in the structural unit. The partial contributions of the M cations, Fe, and Sb are normalized according to the stoichiometry to 3, 12, and 36 modes, respectively.

In general, the spectral weight in the high-energy region ($\hbar\omega>25$ meV) of $Z(\omega)$ is dominated by the Fe contribution while Sb and cation weighted mode intensities are mainly concentrated at energies below 25 meV. However, the cation partial density of states is stretched, at least, over the entire regime of Sb-weighted modes. A pronounced spectral weight in the low-energy range exists for the heavy cation Yb only. In any of the structures, the partial cation dynamics are not characterized by a simple profile. They show a complex texture and an extensive intensity distribution. This holds as well for the low-energy part of the spectra, in which Fe, and, in particular, Sb show textures in the partial spectral distributions reflecting features of, and pointing at a well-established coupling with the cation dynamics. Note, for example, the double-peak feature in the Yb and Sb partial $Z(\omega)$ of $Yb_{1-x}Fe_4Sb_{12}$. Table V offers an overview of all calculated Γ-point energies $[\hbar\omega(Q=0)]$. The data are sorted by energy of the Γ-point modes of $Ba_{1-x}Fe_4Sb_{12}$.

Let us limit our survey to characteristics which can be unequivocally identified in a resolution-limited experiment. Starting with the high-energy modes ($\hbar\omega>25$ meV) we may identify a systematic shift of the Fe dominated bands with smallest and largest values for the Ba- and Yb-hosting structures, respectively. Another shift is associated with the supposed high-energy rim of the Sb band [3 Tg(R) mode around 20 meV] which is appreciably redshifted in

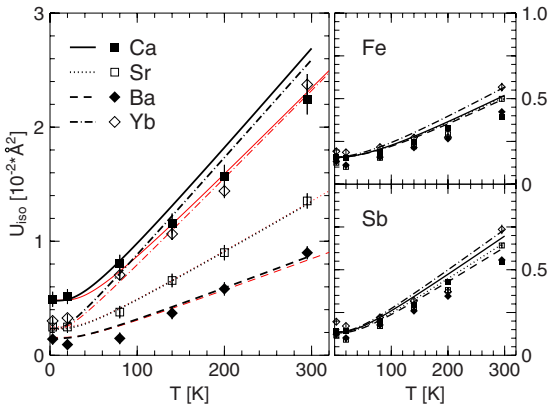

FIG. 4. (Color online) Isotropic thermal parameters $U_{iso}(T)$ as calculated (lines) and obtained from Rietveld fits to neutron-diffraction data (symbols) in filled $M_{1-x}Fe_4Sb_{12}$ skutterudites. $U_{iso}(T)$ of the Ca, Sr, Ba, and Yb cations are shown on the left, and on the right the $U_{iso}(T)$ of the components of the host network Fe (top) and Sb (bottom) are displayed. The corresponding symbols and line codes are given in the left figure. Fits of the Einstein model are shown in red color (same line code).

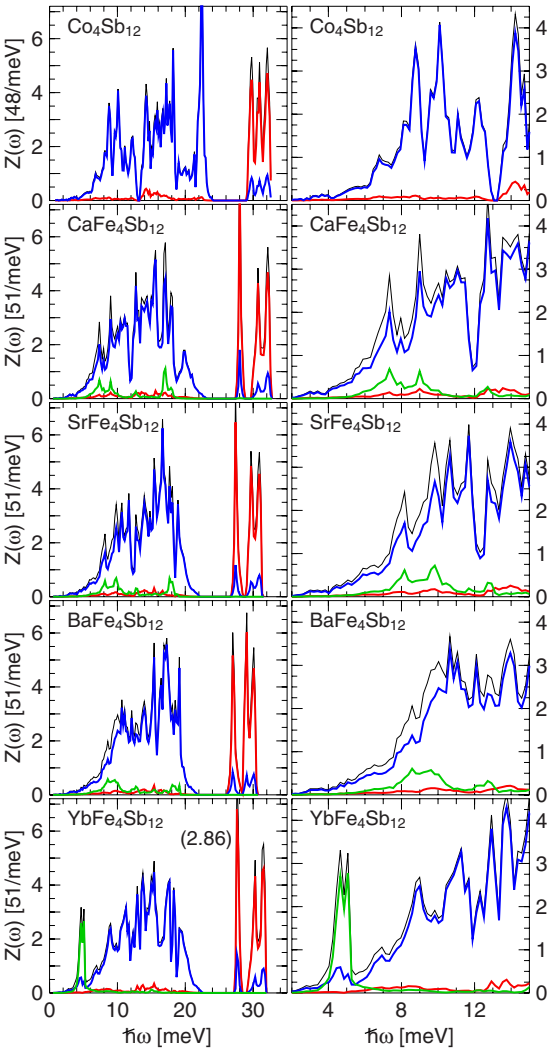

FIG. 5. (Color online) (Left) Vibrational density of states $Z(\omega)$ of the empty skutterudite structure Co_4Sb_{12} and the Ca-, Sr-, Ba-, and Yb-filled skutterudites obtained from *ab initio* lattice-dynamics calculations. (Right) Corresponding $Z(\omega)$ in the energy range of supposed "rattling" modes. Black line represents the total $Z(\omega)$, red the Fe, blue the Sb, and green the M partial density of states, respectively.

TABLE V. Γ-point energies in millielectron volt as obtained from *ab initio* DFT calculations. Eigenfrequencies are ordered with respect to their sequence in $Ba_{1-x}Fe_4Sb_{12}$. Raman (R) and infrared (I) active excitations are marked with the multiplicity and symmetry of the eigenmodes.

Ca	Sr	Ba	Yb	Symmetry
0.0	0.0	0.0	0.0	3 Tu(I)
7.6	8.2	8.6	5.0	3 Tu(I)
11.2	11.4	11.3	11.2	3 Tg(R)
10.9	11.2	11.4	10.6	1 Au
11.5	11.7	11.9	9.8	3 Tu(I)
11.8	12.0	12.4	11.9	3 Tg(R)
12.1	13.9	14.5	11.9	2 Eg(R)
13.9	14.4	14.5	13.8	3 Tu(I)
15.1	15.2	15.2	15.2	2 Eu
16.0	17.0	16.8	15.8	1 Ag(R)
17.4	17.1	16.8	17.6	3 Tg(R)
16.8	17.1	17.1	15.4	3 Tu(I)
17.3	16.9	17.4	17.7	2 Eg(R)
18.4	17.7	18.0	17.9	3 Tu(I)
18.3	17.8	18.4	18.5	1 Ag(R)
20.3	19.9	19.6	20.5	3 Tg(R)
27.3	26.7	26.2	27.4	1 Au
27.4	27.0	26.6	27.3	3 Tu(I)
29.2	29.0	28.6	29.2	3 Tu(I)
31.0	30.4	29.6	31.3	2 Eu
31.7	31.2	30.5	31.9	3 Tu(I)

$Ba_{1-x}Fe_4Sb_{12}$ in comparison to $Yb_{1-x}Fe_4Sb_{12}$.

The most distinct features, however, can be expected in the low-energy part of the spectra ($\hbar\omega < 12.5$ meV) in which Γ-point frequencies appear to be well separated. It is noteworthy here that within the calculated data the Γ-point frequencies cannot account for a number of distinct peaks found in the calculated $Z(\omega)$ shown in Fig. 5. For $Yb_{1-x}Fe_4Sb_{12}$ it is the peak of higher energy at 5 meV only which can be assigned to the IR-active [3 Tu(I)] mode. Peaks at 4.8 meV as well as 7.5 and 9 meV miss an explanation within the Γ-point scheme. Equivalent conclusions can be drawn upon features monitored in the other compounds.

A pictorial presentation of the spectral weight with which the sample constituents contribute to $Z(\omega)$ is given in Fig. 6 which reports the cumulative spectral weight (CSW) defined as

$$N_i(\omega) = \int_0^{\omega} Z_i(\omega')d\omega', \tag{9}$$

with $i=M$ cation, Sb, and Fe and the limit $N_i(\omega \to \infty)=1$.

For a complete equipartition of the dynamics of the constituents of a compound we expect all $N_i(\omega)$ to follow a common profile. For a progressive dynamic decoupling the area spanned between the curves should increase progressively. A strong difference is observed for the Sb and Fe

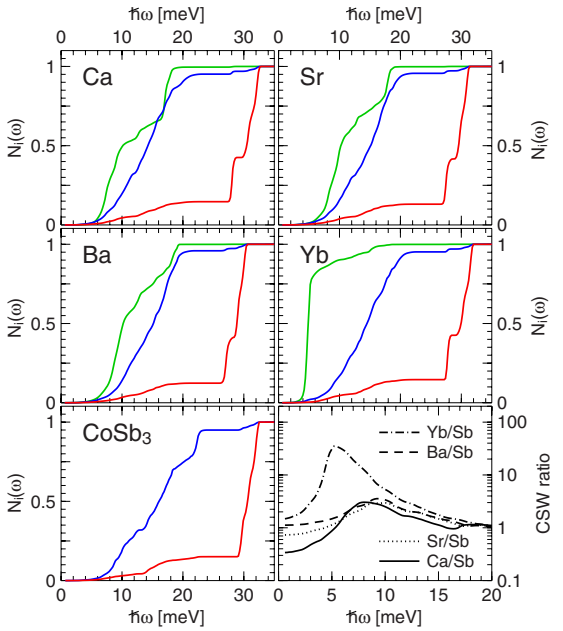

FIG. 6. (Color online) Cumulative spectral weight $N_i(\omega)$ of Ca-, Sr-, Ba-, and Yb-filled $M_{1-x}Fe_4Sb_{12}$ skutterudites computed from density of states reported in Fig. 5. Results on the empty Co_4Sb_{12} structure are plotted for comparison. Samples are characterized in the figures by the M cations. Green line corresponds to the M cation, blue to the Sb, and red to the Fe. Equally shown (right panel, bottom figure) is the cumulative spectral weight (CSW) ratio of M cation to Sb.

dynamics. Throughout all the compounds calculated, about 95% of the Sb CSW is concentrated within the energy range $\hbar\omega < 20$ meV in which only 15% of the Fe contribution can be identified with the remaining 85% within the three strong peaks centered around 30 meV. However, this is a general property of the Fe_4Sb_{12} sublattice and not caused by the presence of a M cation as it is observable in the binary compound $CoSb_3$.

As it can be expected from the properties of $Z_i(\omega)$ a dramatic change is observed for $N_i(\omega)$ of the M cations. In contrast to the $N_i(\omega)$ of Ca, Sr, and Ba showing a close relation to the progression of Sb, $N_i(\omega)$ of Yb separates from the one of Sb. The behavior of Yb can be termed as inversely related to the Fe properties as 85% of the Yb CSW is concentrated within the energy range $\hbar\omega < 6$ meV in which only about 5% of the Sb weight can be identified.

The CSW ratio $N_M(\omega)/N_{Sb}(\omega)$, as it is presented in the bottom right plot of Fig. 6, has a particular virtue for the interpretation of thermodynamic observables which are determined by the total phonon density of states, as indicated by Eq. (7) for the heat capacity. $N_M(\omega)/N_{Sb}(\omega)$ indicates to what extent $C(T)$ is determined by the partial density of states. An equipartition of cation and Sb contributions would correspond to unity. Consequently, below an energy of 5 meV and hence a temperature of about 60 K the heat capacity of a $Ca_{1-x}Fe_4Sb_{12}$ sample is predominantly determined by the dynamics of the Fe_4Sb_{12} matrix. A contrasting behavior has to be noted in the case of $Yb_{1-x}Fe_4Sb_{12}$ in which an Yb contributes 36 times more than a single Sb atom at 5 meV, i.e. 3 times more than the entity of the Sb sublattice. In the

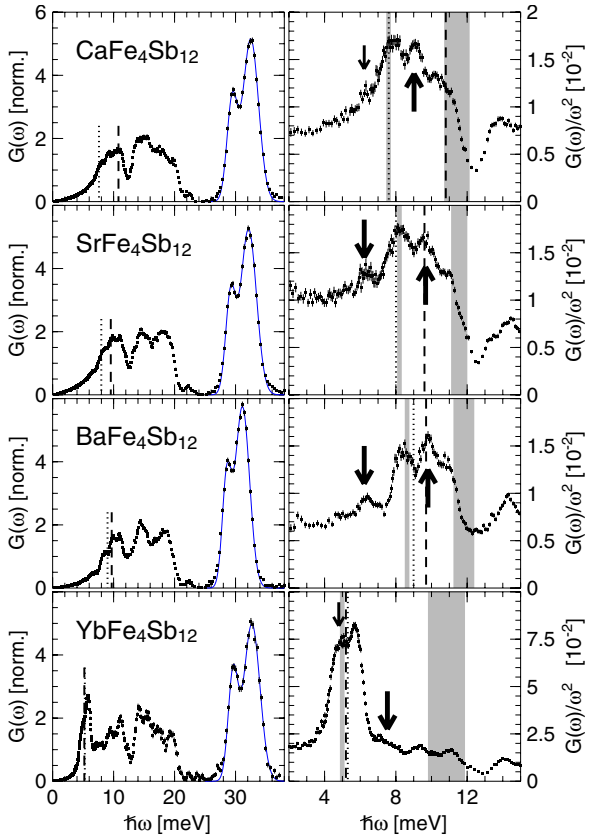

FIG. 7. (Color online) (Left) Generalized density of states $G(\omega)$ of Ca-, Sr-, Ba-, and Yb-filled $M_{1-x}Fe_4Sb_{12}$ skutterudites measured at IN6@ILL at $T=300$ K. Dashed line and dotted line correspond to the Einstein mode energy $\omega_{i,E}$ conjectured from the ADPs of neutron-diffraction data reported in Table VI and specific heat reported in Ref. 20, respectively. Blue full line represents Gaussian fits to the high energy modes. (Right) Debye presentation $G(\omega)/\omega^2$ of the corresponding data sets. Gray shaded areas indicate energy regions for which *ab initio* lattice-dynamics calculations anticipate a strong contribution from Γ-point excitations reported in Table V. Vertical arrows indicate mode peaks which cannot be accounted for by Γ-point excitation scheme. Dashed and dotted lines indicate the Einstein mode energy as in the left column. Note the close resemblance of the optic Γ-point [3 Tu(I)] mode of lowest energy to the Einstein mode energy conjectured from specific heat data (Ref. 20).

cases of Sr and Ba filled structures the contributions to $C(T)$ from a M cation and a single Sb atom are rather equilibrated.

D. Time-of-flight neutron-scattering experiments and the generalized density of states

The generalized density of states $G(\omega)$ computed from IN6@ILL measurements is presented in Fig. 7. The overall $G(\omega)$ profile is characterized by the idiosyncratic mode gap ($\sim$20–28 meV) separating the two bands of dominant M-Sb ($\hbar\omega<20$ meV) and Fe ($\hbar\omega>28$ meV) inelastic signals. Within the high-energy Fe mode regime the two peaks of highest energy (see Fig. 5) could not be resolved in the experiment. For a quantitative comparison with the calculation results the Fe modes are fitted with two Gaussian functions. The positions of the calculated and fitted data are presented

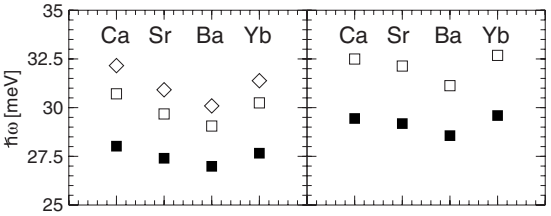

FIG. 8. (Left) Energy of the Fe dominated modes in Ca-, Sr-, Ba-, and Yb-filled MFe_4Sb_{12} skutterudites as computed from *ab initio* lattice-dynamics calculations (Fig. 5). (Right) Fe mode energies obtained from Gaussian fits to experimental $G(\omega)$ (Fig. 7). Note that the high-energy double peak is not resolved in the experiment.

in Fig. 8. Note that the iron mode redshift taking on a minimum in $Ba_{1-x}Fe_4Sb_{12}$ is congruently observed in experiment and calculation. As expected from the calculation results a slight redshift of the Ba-Sb weighted band (see Fig. 5) can be confirmed.

The low-energy regime of $G(\omega)$ is bound by a shallow minimum around 12–14 meV. Ca, Sr, and Ba hosting structures show an apparently similar $G(\omega)$ profile in this energy range. A clear departure in the form of a pronounced double peak at the low-energy side of the data is observed with the $Yb_{1-x}Fe_4Sb_{12}$ sample. Since this low-energy part of $G(\omega)$ has crucial influence on the specific heat of the samples and the ADPs of the elements, we have indicated for comparison Einstein mode energies as they could be approximated from ADPs presented in Fig. 4 (dashed line) and from $C(T)$ measurements (dotted line).[20]

The important points to be highlighted here are, on the one hand, the converging trend of the Einstein mode energies from ADP and $C(T)$ data upon increasing the mass of the cation, and on the other, the overall close resemblance of the Γ-point 3 Tu(I) mode with the Einstein mode energy conjectured from $C(T)$ data. For Ba and Yb a perfect match of the Γ-point 3 Tu(I) energy, the Einstein mode energy from $C(T)$ and the cation mode energy from ADP is found.

A closeup look at the details of this energy range is offered by the Debye plot $G(\omega)/\omega^2$ in the right column of Fig. 7. Such a plot points out sensitively any inelastic intensity which is not due to acoustic phonons in the long-wavelength regime $\hbar\omega(Q)\propto Q$. The numerous peaks on the $G(\omega)/\omega^2$ data stem from van Hove singularities at which the phonon group velocity $d\omega(Q)/dQ\approx 0$. All peaks identified from $G(\omega)/\omega^2$ are summarized in Table VI.

To discriminate intensity maxima due to localized optic modes in the vicinity of the Γ point from peaks created by the dispersive characteristics of the phonons away from zone center the gray shaded areas indicate energy ranges in which a cumulation of zone-center modes is calculated (see Table V). Also sketched are the Einstein mode energies estimated from ADPs of the cations and from specific heat.

Peaks which cannot be explained within the calculated data are marked by vertical arrows. An obvious feature common to all samples is the peak at 9–10 meV. Its origin is very likely a zone-boundary signal from dispersive optic sheets as it is not represented by any of the calculated zone center modes listed in Table V. Another striking property of Sr-,

TABLE VI. Characteristic peak energies in millielectron volt identified in $G(\omega)$ data and Einstein mode energies of the M cations conjectured from calculated potentials ($\omega_{i,\mathrm{R}}$, Eq. (6)) reported in Table IV, from fitted ADPs ($\omega_{i,\mathrm{E}}$, Eq. (5)) reported in Fig. 4 and from specific heat [$c(T)$] data of Ref. 20. The compounds $M_{1-x}Fe_4Sb_{12}$ are characterized by the cations.

	Ca	Sr	Ba	Yb
$G(\omega)/\omega^2$		6.5	6.5	4.9
				5.7
	8.0	8.2	8.4	7.5
	9.2	9.9	9.9	9.4
	11.5	11.1	10.9	11.1
$\omega_{i,\mathrm{R}}$	9.6	8.8	8.8	4.6
$\omega_{i,\mathrm{E}}$	10.8(1)	9.61(3)	9.7(6)	5.2(2)
$c(T)$	7.6	8.0	9.0	5.3

Ba-, and Yb-filled compounds is the first low-energy peak. It is obvious that for Sr and Ba it cannot be assigned to the zone-center [3 Tu(I)] mode either. Note that the double-peak characteristics in Yb data is a real feature observed in the high-resolution experiment and reproduced by the calculation shown in Fig. 5, however, shifted to lower energies by about 1 meV in the computer results. Consequently, the calculated zone-center [3 Tu(I)] mode corresponds to the second peak of the calculated $Z(\omega)$ and to the second peak of the measured $G(\omega)$. Its behavior is, hence, in line with the Sr and Ba data and the low-energy peak not explained by Γ-point excitations marked with a small vertical arrow. A discrepancy from this universal inelastic feature is formed by the dynamics of $Ca_{1-x}Fe_4Sb_{12}$ in which only a strong optic peak dominates the spectral distribution. This, however, is an apparent characteristic only as the intensity of a number of modes in the low-energy region is merged and cannot be resolved experimentally. We will address this point in full detail in a forthcoming publication on phonon dispersion phenomena. A small arrow indicates the hypothetical peak position.

The origin of the first peak in $G(\omega)$ is the localization $d\omega(Q)/dQ \approx 0$ of phonon sheets in the vicinity of the zone boundary as it has been elaborated in full detail for the case of $LaFe_4Sb_{12}$.[29–31,34] Taking into account the scattering powers of the elements Sr and Ba which differ by a factor of 3, the rather similar intensity of the experimental $G(\omega)$ of $Sr_{1-x}Fe_4Sb_{12}$ and $Ba_{1-x}Fe_4Sb_{12}$ indicates a pronounced spectral weight of Sb in the low-energy phonon sheets. It is noticeable that the Einstein mode energy derived from the cation ADP data reflects the average value of the two low-energy peaks in the $Yb_{1-x}Fe_4Sb_{12}$ spectra as it is the case for $LaFe_4Sb_{12}$ data.[34] As they are dominated by the M-cation contribution we may conjecture that the ADP results reflect to a good approximation as well the averaged behavior of the M mode distribution in the low-energy part of Ca, Sr, and Ba.

E. Specific heat

The precision of the calculated $Z(\omega)$ can be crosschecked experimentally by the heat capacity $C(T)$ or specific-heat

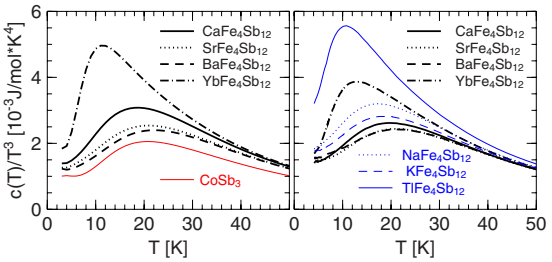

FIG. 9. (Color online) (Left) Specific heat $c(T)/T^3$ of Ca-, Sr-, Ba-, and Yb-filled MFe_4Sb_{12} and of $CoSb_3$ calculated from *ab initio* lattice-dynamics data. (Right) Measured $c_p(T)/T^3$ of Ca-, Sr-, Ba-, and Yb-, as well as, of Na-, K-, and Tl-filled $M_{1-x}Fe_4Sb_{12}$ skutterudites. Experimental data are taken from Refs. 20 and 64 and correspond to the vibrational contribution of the lattice to the specific heat.

$c(T)$ behavior. The results are plotted in Fig. 9. The plot on the left-hand side reports the calculated $c_V(T)$ and the plot on the right-hand side indicates measured $c_p(T)$ data, whereby we assume $c(T)=c_V(T)\approx c_p(T)$ which is justified for such low temperatures. Results on Na-, K-, and Tl-filled $M_{1-x}Fe_4Sb_{12}$ skutterudites are indicated for comparison.[20,64] The presentation $c(T)/T^3$ vs T stresses the low-energy, low-temperature regime dominated supposedly by the M-cation dynamics.

In general, a good correspondence can be identified between calculated and measured data on an absolute scale. This statement holds to a high degree for Sr- and Ba-filled structures. In the case of Ca- and Yb-filled iron antimonides the calculation overestimates the low-temperature $c(T)$. However, as for the Yb compound an excess $c(T)$ should be expected from the properties of $Z(\omega)$ in which the M-cation modes are calculated at lower energies than experimentally found in $G(\omega)$. On an absolute scale, the calculated $c(T)/T^3$ of $Yb_{1-x}Fe_4Sb_{12}$ approaches the measured values of the thallium containing skutterudite.

The $c(T)$ excess in the Ca-filled compound has a different origin which is substantiated by the partial contributions depicted in Fig. 10. In comparison to Ba, Ca contributes less to $c(T)$, however, the Sb atoms of the $Ca_{1-x}Fe_4Sb_{12}$ host matrix are augmenting the $c(T)$ beyond the one of $Ba_{1-x}Fe_4Sb_{12}$ and, hence, of $Sr_{1-x}Fe_4Sb_{12}$. Such an excess is less evident in the experimental data (Fig. 9), however, it is detectable.

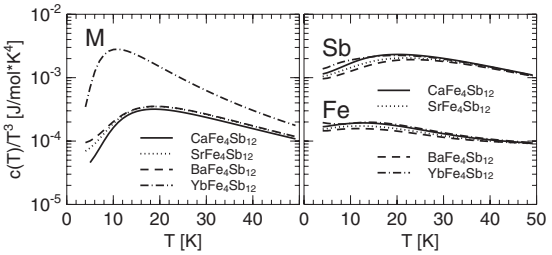

FIG. 10. (Left) Partial specific heat $c(T)/T^3$ of Ca-, Sr-, Ba-, and Yb-filled $M_{1-x}Fe_4Sb_{12}$ skutterudites calculated from *ab initio* lattice-dynamics data. (Right) Partial specific heat $c(T)/T^3$ of Sb and Fe/Co in $Ca_{1-x}Fe_4Sb_{12}$, $Sr_{1-x}Fe_4Sb_{12}$, $Ba_{1-x}Fe_4Sb_{12}$, and $Yb_{1-x}Fe_4Sb_{12}$ and Co_4Sb_{12}.

IV. DISCUSSION

As we have pointed out in Sec. III A the link among the studied observables is the collective vibrational dynamics of the skutterudite compounds which may be related, for a harmonic system, to a temperature-independent phonon density of states $Z(\omega)$. As for the calculated data the computation of $Z(\omega)$, of atomic displacement parameters $U_{\mathrm{iso}}(T)$ and of specific heat $c(T)$, and their interpretation is a facile task. The comprehension of experimentally obtained data necessitates, however, some caution.

For example, experimental $U_{\mathrm{iso}}(T)$ are obtained from fit procedures to diffraction data with a complexity of correlated fit parameters. An additional uncertainty in experimental data is given by the presence of defects. Consequently, we might expect good comparative results whose dependence on the M cation and temperature variation should be well reflected within the experimental and calculated $U_{\mathrm{iso}}(T)$. On an absolute scale we might not expect a perfect match *ad hoc*. Nonetheless, the isotropic displacement parameters of the cations from experiment and calculation are in good agreement and their dependence on cation variation and T well reproduced (Fig. 4). Yb and Ca, respectively, display higher $U_{\mathrm{iso}}(T)$ than Sr and, in particular, Ba.

A direct observation of the influence of different M cations on the host potential is offered by the experimentally determined density of states $G(\omega)$. The measured variation in the position of the strong Fe peaks around 30 meV is a fingerprint of the ionic interaction between the cations M and the polyanion Fe_4Sb_{12} and reproduced by the calculated $Z(\omega)$ (cf. Fig. 8). A gross influence on eigenmodes with a strong Sb participation can be easily deduced from the shift of the high-energy band edge from 20 meV in Ca towards 19 meV in Ba containing compounds. Experimental and calculation data are as well in good agreement.

Closer inspection of the Sb band data is complicated by the coherent scattering character and the alternating scattering powers of the M cations leading to the generalized response $G(\omega)$. Unequivocal conclusions can be, however, drawn from the low-energy data at $\hbar\omega \leq 13$ meV which are dominated by a few phonon modes only resulting in peaks in $G(\omega)$ well separated in energy and, hence, distinguishable in resolution influenced experiments. An important property of the low-energy region is that the number of peaks neither in $Z(\omega)$ nor in $G(\omega)$ can be explained by the Γ-point excitations $\hbar\omega(Q=0)$ which are listed in Table V. This result should not come as a surprise, since peaks in the density of states are due to van Hove singularities of the phonon system and, hence, created by any mode whose group velocity $d\omega/dQ \approx 0$ at some point in the ω-Q phase space. This holds, for example, for acoustic modes close to the Brillouin-zone boundary in a simple structure of cubic symmetry.

The acoustic and low-energy phonon sheets are not exclusively determined by the M-cation dynamics as it might be conjectured from the enhanced ADPs. A comparison of $G(\omega)$ of Sr and Ba whose scattering powers differ by a factor of 3 indicates that Sb motions contribute substantially to the acoustic intensities. Such a conclusion is substantiated by the partial contributions to $Z(\omega)$, and a comparison of the calculated spectral weight ratio as it is presented in Fig. 6 indicates that the light filler cations Ca, Sr as well as Ba do not play a dominant role for the specific heat $c(T)$ of the skutterudite systems. Indeed, the contribution of Ca to $c(T)$ appears to be irrelevant in consideration of the respective Sb contribution as it is evidenced by the partial components reported in Fig. 10. Only the $c(T)$ of Yb-filled structures, in which the spectral weight of the M cation is concentrated at low energies, is rather determined by its dynamics.

A matching picture has been conjectured from experimental data[20] which indicate a nonconformity of Einstein frequencies extracted from $c(T)$ measurements and $U_{\mathrm{iso}}(T)$ data for the light cations and fully supported by the Einstein mode energies computed from the here reported neutron-diffraction results. These modes are listed in Table VI and graphically indicated in Fig. 7. The mismatch of Einstein frequencies from ADP and $c(T)$ results is dramatically manifested in Ca, and well obvious in Sr comprising structures. It is only lifted for the Yb case.

As a consequence of the entire body of results presented here and in Ref. 20 we have to conclude that the atomic displacement parameters of the M cations in $M_{1-x}Fe_4Sb_{12}$ are not solely representative for the thermal properties of the skutterudite compounds. In comparison to the properties of Sb light atoms such as Ca, Na, or K may show enhanced $U_{\mathrm{iso}}(T)$, but their partial density of states $Z_i(\omega)$ at low energies is too small to dictate the properties of $c(T)$ of the iron antimonide compounds. Some significance of the Einstein frequency approximated from $c(T)$ can be found within its good correspondence with the optic mode of lowest energy [3 Tu(I)] and, in the case of the heavy Yb, to some extent with the average position of the eigenmodes dominated by the cation. This should be expected on intuitive grounds since due to the Bose-Einstein statistics of phonons the low-energy van Hove singularities are the leading terms in $c(T)$ experiments at low and moderate temperatures as it is approximated by Eq. (7).

From a different point of view we may conclude and stress that large $U_{\mathrm{iso}}(T)$ do not exclude a strong participation of the M cations to modes at high energies. This statement is best evidenced in the partial $Z(\omega)$ of the light guests which show a strong spectral weight in the range of 16–18 meV. For example, about 35% of the Ca and 25% of the Sr spectral weight is to be found in this range, as indicated by $N_i(\omega)$ in Fig. 6. The elevated Einstein mode frequency obtained from the $U_{\mathrm{iso}}(T)$ of the light cations is another manifestation of their contribution to eigenmodes at higher energies and a consequence of Eq. (4) leading for the Einstein model to the relation $\langle u_i^2(T)\rangle_{T\to\infty} \propto 1/(M_i \cdot \omega_{i,\mathrm{E}}^2)$.

Results on $La/CeFe_4Sb_{12}$ (Refs. 31 and 34) as well as $TlFeCo_3Sb_{12}$ (Ref. 32) are in line with and complementary to the data presented here. The conform behavior comprises as well the trend of the DFT results when compared with experimental data to underestimate force constants and, hence, eigenfrequencies and to overestimate the localization of the low-energy normal modes. This can be best viewed, for example, in the computed $U_{\mathrm{iso}}(T)$ of Ca and Yb and the $c(T)$ data of $Ca_{1-x}Fe_4Sb_{12}$ and $Yb_{1-x}Fe_4Sb_{12}$ exceeding the experimental results. The generally lowered peak positions of the Fe-weighted modes in $Z(\omega)$ is another manifestation of the underestimated force constants in our DFT calculations. Not

much attention has been paid in the current publication to this consistent trend since temperature effects on the dynamics of the filled iron antimonides have to be inspected experimentally before an adequate discussion can be made. Temperature effects will be addressed in a forthcoming paper.

The data presented here indicate that there is no need to introduce any additional random component into the dynamics of the studied compounds that might reflect some randomly disordered nature of a glass. It is necessary, however, to note that pronounced partial filling, the application of misch-metal cations and/or the variation in the chemical composition by atomic substitution within the anion lattice introduce such a disordered, glassy component into the dynamics and, hence, into the mechanism reducing the lattice thermal conductivity in skutterudites.[10,11,18,27,37,65–72]

The present data demonstrate as well that the often reported low-energy Einstein mode in materials comprising heavy M cations could be a result of resolution limited experiments. Adopting the terminology of Einstein modes, we have to conclude even for the case of $Yb_{1-x}Fe_4Sb_{12}$ that there exist at least two Yb-weighted Einstein modes, one at 4.9 meV and the other at 5.7 meV. Only a spectrometer with an energy resolution of less than 200 μeV enables us to make this statement. The appreciably lowered energy of the Yb-weighted modes is not a result of the Yb mass only but determined as well by weaker restoring forces as computed from the potential energy calculations (cf. Fig. 3 and Table IV).

V. SUMMARY AND OUTLOOK

The present paper reports on results from time-of-flight neutron spectroscopy, neutron diffraction, specific-heat experiments and *ab initio* lattice-dynamics calculations on the ternary skutterudites $Ca_{1-x}Fe_4Sb_{12}$, $Sr_{1-x}Fe_4Sb_{12}$, $Ba_{1-x}Fe_4Sb_{12}$, and $Yb_{1-x}Fe_4Sb_{12}$. We show that the vibrational dynamics of the compounds display the lattice dynamics of quasiharmonic crystals, with the M cations forming collective, hybrid modes with the Fe_4Sb_{12} matrix. The distribution of eigenfrequencies and the partial amplitudes with which the compound constituents contribute to them is computable to a satisfactory degree.

The good correspondence of experimental and calculated data does not only comprise the vibrational density of states but also material properties linked to the vibrational properties within the framework of the Debye theory. These are, the atomic displacement parameters $U_{iso}(T)$ and the specific heat $c(T)$. $U_{iso}(T)$ and $c(T)$ are computed within the harmonic approximation from $Z(\omega)$ for $T=0$ K, however, they reflect closely the properties of the measured data which have been obtained *in situ* on temperature variation between 3 and 295 K. This match indicates that anharmonic effects are not affecting the dynamics of the samples significantly in the temperature range applied.

The calculation of partial contributions of the compound constituents offers a deeper insight into their dynamic interplay. Hence, an explanation is given for the reduced significance of the lighter cations for the total $c(T)$ of the samples despite their elevated $U_{iso}(T)$.

So far temperature effects on the inelastic response of the compounds and the detailed dispersion of phonons have not been considered in detail. These points will be addressed in a forthcoming publication.

ACKNOWLEDGMENTS

The authors thank Karin Kreutziger for help and technical support with the sample preparation. The ILL College 7 is acknowledged for the support of this work and the grant of accessing the instruments of the European neutron source Institut Laue Langevin. L.C. and M.M.K. acknowledge with appreciation the free access to ILL's "Scientific Computing" facility.

[1] I. Oftedal, Z. Kristallogr. **66**, 517 (1928).
[2] A. Kjekshus and T. Rakke, Acta Chem. Scand., Ser. A **28a**, 99 (1974).
[3] W. Jeitschko and D. Braun, Acta Crystallogr., Sect. B: Struct. Crystallogr. Cryst. Chem. **33**, 3401 (1977).
[4] B. C. Sales, B. Mandrus, and R. K. Williams, Science **272**, 1325 (1996).
[5] B. C. Sales, D. Mandrus, B. C. Chakoumakos, V. Keppens, and J. R. Thompson, Phys. Rev. B **56**, 15081 (1997).
[6] G. J. Snyder and E. S. Toberer, Nature Mater. **7**, 105 (2008).
[7] D. M. Rowe, *CRC Handbook of Thermoelectrics* (CRC, Boca Raton, 1995).
[8] G. S. Nolas, J. Sharp, and H. J. Goldsmid, *Thermoelectrics Basic Principles and New Materials Developments* (Springer, New York, 2001).
[9] G. S. Nolas, D. T. Morelli, and T. M. Tritt, Annu. Rev. Mater. Sci. **29**, 89 (1999).
[10] G. P. Meisner, D. T. Morelli, S. Hu, J. Yang, and C. Uher, Phys. Rev. Lett. **80**, 3551 (1998).
[11] G. S. Nolas, J. L. Cohn, and G. A. Slack, Phys. Rev. B **58**, 164 (1998).
[12] G. A. Slack and V. G. Tsoukala, J. Appl. Phys. **76**, 1665 (1994).
[13] G. S. Nolas, J. L. Cohn, G. A. Slack, and S. B. Schujman, Appl. Phys. Lett. **73**, 178 (1998).
[14] J. S. Tse and M. A. White, J. Phys. Chem. **92**, 5006 (1988).
[15] J. S. Tse, V. P. Shpakov, V. R. Belosludov, F. Trouw, Y. P. Handa, and W. Press, Europhys. Lett. **54**, 354 (2001).
[16] N. J. English and J. S. Tse, Phys. Rev. Lett. **103**, 015901 (2009).
[17] N. J. English, J. S. Tse, and D. J. Carey, Phys. Rev. B **80**, 134306 (2009).
[18] B. C. Sales, B. C. Chakoumakos, and D. Mandrus, Phys. Rev. B **61**, 2475 (2000).
[19] D. Cao, F. Bridges, P. Chesler, S. Bushart, E. D. Bauer, and M. B. Maple, Phys. Rev. B **70**, 094109 (2004).
[20] W. Schnelle, A. Leithe-Jasper, H. Rosner, R. Cardoso-Gil, R. Gumeniuk, D. Trots, J. A. Mydosh, and Y. Grin, Phys. Rev. B

77, 094421 (2008).
[21] V. Keppens, D. Mandrus, B. C. Sales, B. C. Chakoumakos, P. Dai, R. Coldea, M. B. Maple, D. A. Gajewski, E. J. Freeman, and S. Bennington, Nature (London) **395**, 876 (1998).
[22] R. P. Hermann, R. Jin, W. Schweika, F. Grandjean, D. Mandrus, B. C. Sales, and G. J. Long, Phys. Rev. Lett. **90**, 135505 (2003).
[23] R. Viennois, L. Girard, D. Ravot, H. Mutka, M. Koza, F. Terki, S. Charar, and J.-C. Tedenac, Physica B **350**, E403 (2004).
[24] R. Viennois, L. Girard, M. M. Koza, H. Mutka, D. Ravot, F. Terki, S. Charar, and J.-C. Tedenac, Phys. Chem. Chem. Phys. **7**, 1617 (2005).
[25] G. J. Long, R. P. Hermann, F. Grandjean, E. E. Alp, W. Sturhahn, C. E. Johnson, D. E. Brown, O. Leupold, and R. Ruffer, Phys. Rev. B **71**, 140302(R) (2005).
[26] H.-C. Wille, R. P. Hermann, I. Sergueev, O. Leupold, P. van der Linden, B. C. Sales, F. Grandjean, G. J. Long, R. Ruffer, and Y. V. Shvyd'ko, Phys. Rev. B **76**, 140301(R) (2007).
[27] Y. Wang, X. Xu, and J. Yang, Phys. Rev. Lett. **102**, 175508 (2009).
[28] J. L. Feldman and D. J. Singh, Phys. Rev. B **53**, 6273 (1996).
[29] J. L. Feldman, D. J. Singh, I. I. Mazin, D. Mandrus, and B. C. Sales, Phys. Rev. B **61**, R9209 (2000).
[30] J. L. Feldman, D. J. Singh, C. Kendziora, D. Mandrus, and B. C. Sales, Phys. Rev. B **68**, 094301 (2003).
[31] J. L. Feldman, P. Dai, T. Enck, B. C. Sales, D. Mandrus, and D. J. Singh, Phys. Rev. B **73**, 014306 (2006).
[32] P. Ghosez and M. Veithen, J. Phys.: Condens. Matter **19**, 096002 (2007).
[33] M. M. Koza, M. R. Johnson, R. Viennois, H. Mutka, L. Girard, and D. Ravot, in Proceedings of ICT'06, 25th International Conference on Thermoelectrics 2006 (IEEE-CPMT, Piscataway, NJ, 2007), 06TH8931, p. 70.
[34] M. M. Koza, M. R. Johnson, R. Viennois, H. Mutka, L. Girard, and D. Ravot, Nature Mater. **7**, 805 (2008).
[35] H. Schober, H. Itoh, A. Klapproth, V. Czihaia, and W. F. Kuhs, Eur. Phys. J. E **12**, 41 (2003).
[36] M. M. Koza and H. Schober, in *Vibrational Dynamics and Guest-Host Coupling in Clthrate Hydrates*, Neutron Scattering Applications and Techniques (Springer, New York, 2009).
[37] C. P. Yang, H. Wang, K. Iwasa, M. Kohgi, H. Sugawara, and H. Sato, Appl. Phys. Lett. **90**, 102503 (2007).
[38] C. P. Yang, H. Wang, K. Iwasa, M. Kohgi, H. Sugawara, and H. Sato, J. Phys.: Condens. Matter **19**, 226214 (2007).
[39] C. H. Lee, I. Hase, H. Sugawara, H. Yoshizawa, and H. Sato, J. Phys. Soc. Jpn. **75**, 123602 (2006).
[40] K. Iwasa, M. Kohgi, H. Sugawara, and H. Sato, Physica B **378-380**, 194 (2006).
[41] K. Iwasa, Y. Mori, L. Hao, Y. Murakami, M. Kohgi, H. Sugawara, and H. Sato, J. Phys.: Conf. Ser. **92**, 012122 (2007).
[42] S. Tsutsui, H. Kobayashi, D. Ishikawa, J. P. Sutter, A. Q. R. Baron, T. Hasegawa, N. Ogita, M. Udagawa, Y. Yoda, H. Onodera, D. Kikuchi, H. Sugawara, C. Sekine, I. Shirotani, and H. Sato, J. Phys. Soc. Jpn. **77**, 033601 (2008).
[43] Y. Takasu, T. Hasegawa, N. Ogita, M. Udagawa, M. A. Avila, K. Suekuni, I. Ishii, T. Suzuki, and T. Takabatake, Phys. Rev. B **74**, 174303 (2006).
[44] M. Christensen, A. B. Abrahamsen, N. B. Christensen, F. Juranyi, N. H. Andersen, K. Lefmann, J. Andreasson, C. R. H. Bahl, and B. B. Iversen, Nature Mater. **7**, 811 (2008).
[45] B. Chazallon, H. Itoh, M. Koza, W. F. Kuhs, and H. Schober, Phys. Chem. Chem. Phys. **4**, 4809 (2002).
[46] H. Mutka, M. M. Koza, M. R. Johnson, Z. Hiroi, J.-I. Yamaura, and Y. Nagao, Phys. Rev. B **78**, 104307 (2008).
[47] P. E. Blöchl, Phys. Rev. B **50**, 17953 (1994).
[48] P. Hohenberg and W. Kohn, Phys. Rev. **136**, B864 (1964).
[49] W. Kohn and L. J. Sham, Phys. Rev. **140**, A1133 (1965).
[50] G. Kresse and J. Furthmueller, Comput. Mater. Sci. **6**, 15 (1996).
[51] G. Kresse and D. Joubert, Phys. Rev. B **59**, 1758 (1999).
[52] J. P. Perdew, K. Burke, and M. Ernzerhof, Phys. Rev. Lett. **77**, 3865 (1996).
[53] J. P. Perdew, K. Burke, and M. Ernzerhof, Phys. Rev. Lett. **78**, 1396 (1997).
[54] K. Parlinski, Software PHONON, 2003.
[55] K. Parlinski, Z.-Q. Li, and Y. Kawazoe, Phys. Rev. Lett. **78**, 4063 (1997).
[56] M. R. Johnson, M. M. Koza, L. Capogna, and H. Mutka, Nucl. Instrum. Methods Phys. Res. A **600**, 226 (2009).
[57] W. Schnelle, A. Leithe-Jasper, M. Schmidt, H. Rosner, H. Borrmann, U. Burkhardt, J. A. Mydosh, and Y. Grin, Phys. Rev. B **72**, 020402(R) (2005).
[58] M. M. Koza, Phys. Rev. B **78**, 064303 (2008).
[59] S. W. Lovesey, *Theory of Neutron Scattering from Condensed Matter* (Oxford Science Publications, Oxford, UK, 1984).
[60] G. L. Squires, *Introduction to the Theory of Thermal Neutron Scattering* (Dover Publications, Mineola, New York, 1996).
[61] R. D. Shannon, Acta Crystallogr., Sect. A: Cryst. Phys., Diffr., Theor. Gen. Crystallogr. **32**, 751 (1976).
[62] J. Rodríguez-Carvajal, Physica B **192**, 55 (1993).
[63] N. D. Ashcroft and N. W. Mermin, *Solid State Physics* (Saunders College, Philadelphia, USA, 1976).
[64] A. Leithe-Jasper, W. Schnelle, H. Rosner, R. Cardoso-Gil, M. Baenitz, J. A. Mydosh, Y. Grin, M. Reissner, and W. Steiner, Phys. Rev. B **77**, 064412 (2008).
[65] B. Chen, J.-H. Xu, C. Uher, D. T. Morelli, G. P. Meisner, J.-P. Fleurial, T. Caillat, and A. Borshchevsky, Phys. Rev. B **55**, 1476 (1997).
[66] G. S. Nolas, M. Kaeser, R. T. Littleton, and T. M. Tritt, Appl. Phys. Lett. **77**, 1855 (2000).
[67] J. Yang, D. T. Morelli, G. P. Meisner, W. Chen, J. S. Dyck, and C. J. Uher, Phys. Rev. B **67**, 165207 (2003).
[68] J. G. A. Lamberton, R. H. Tedstrom, T. M. Tritt, and G. S. Nolas, J. Appl. Phys. **97**, 113715 (2005).
[69] M. Puyet, C. Candolfi, L. Chaput, V. DaRos, A. Dauscher, B. Lenoir, and J. Hejtmanek, J. Phys.: Condens. Matter **18**, 11301 (2006).
[70] X. Tang, H. L. Li, Q. Zhang, M. Niino, and T. Goto, J. Appl. Phys. **100**, 123702 (2006).
[71] J. Yang, G. P. Meisner, C. J. Rawn, H. Wang, B. C. Chakoumakos, J. Martin, G. S. Nolas, B. L. Pedersen, and J. K. Stalick, J. Appl. Phys. **102**, 083702 (2007).
[72] J. Y. Peng, P. N. Alboni, J. He, B. Zhang, Z. Su, T. Holgate, N. Gothard, and T. M. Tritt, J. Appl. Phys. **104**, 053710 (2008).